Jurnal Arsip Rekayasa Sipil dan Perencanaan 5(2), 138-148 (2022)
https://doi.org/10.24815/jarsp.v5i2.25766


**Jurnal Arsip Rekayasa Sipil dan Perencanaan (JARSP)**
*Journal of Archive in Civil Engineering and Planning*
E-ISSN: 2615-1340; P-ISSN: 2620-7567

**Journal homepage:** http://www.jurnal.unsyiah.ac.id/JARSP/index

# STRUCTURAL EVALUATION ON PEDESTRIAN BRIDGE CONSTRUCTED OF TRUSS STRUCTURE AND CASTELLATED BEAM

**Arief Panjaitan**[a,*]
[a]Civil Engineering Department, Syiah Kuala University, Banda Aceh 23111, Indonesia
**Corresponding author,* email address: arief_panjaitan@unsyiah.ac.id

ARTICLE INFO

*Article History:*
Received 25 April 2022
Accepted 18 May 2022
Online 31 June 2022

*Keywords:*
Structural evaluation
Pedestrian bridge
Truss structure
Castellated beam
Internal force
Deflection

ABSTRACT

A pedestrian bridge is a structure linking a pedestrian or bike path over or around a major roadway, railway, or waterway. The truss bridge (TRB) and the bridge with a castellated beam (CBB) are the common models of the pedestrian bridge. Past studies have revealed the structural behavior of TRB and CBB, but the performances of both bridges have not yet been comparatively confirmed. This study examined the TRB and CBB structural performances to obtain the better bridge model due to applied loading. The research was started by establishing the bridge models and employing the load combinations. The analysis resulted in the internal forces and they were used to design the bridges. The design is referred to as the SNI-1729-2020. This research revealed that the TRB exhibited structural performances, i.e., deflection and internal force, better than those of the CBB. Nevertheless, due to the many steel members, the TRB presented a heavier bridge than the CBB.



## 1. INTRODUCTION

Pedestrian bridges are an essential part of urban road projects. This type of bridge is typically built in high-traffic areas to assist people in crossing the street and to facilitate contact between buildings. So far, several studies have been conducted. Li (2011) investigated the finite element model of a pedestrian bridge by using irregular vibration analysis. In that research work, irregular vibrations were distinguished by referring to their causes, i.e., light rail, vehicles, and walking pedestrians.

Dey et al. (2015) provided a serviceability assessment of two full-scale aluminum pedestrian bridges with different vibration characteristics. The evaluations of the two bridges were performed by comparing the measurements with the predicted and acceptable limits of vibrations as recommended in codes and several guidelines. Ali et al. (2020) developed a pedestrian suspension bridge with a new type of composite deck using Glass Fibre Reinforced Polymer (GFRP). Belykh et al. (2017) investigated pedestrian phase-locking due to footstep phase adjustment, suspected to be the main cause of its large lateral vibrations. They developed foot force models of pedestrians' responses to bridge motion and detailed Kustura et al. (2020) conducted the tests on several pedestrian bridges. The scope of testing was determined depending on the geometric and calculation characteristics of the tested structure and the legal regulations.

Chang-jun et al. (2011) analytically evaluated the 75-meter-mountainous bridge main span to carry on analysis respectively for the cable-truss bridge, suspension bridge, and suspended bridge. Sophocleous-Lemonari et al. (2013) exemplified the process of the design of a pedestrian steel bridge with a span of 60 m aiming at self-weight minimization and construction standardization. Li et al. (2013) studied the effect of wind pressure on pedestrian bridges induced by mainline trains. This has been investigated using numerical simulation. Tej et al. (2014) presented the design of an experimental tensegrity pedestrian bridge. The structure was designed as a permanent, three-span bridge.

Wackcaure et al. (2012) researched the castellated beams and they were found to be efficient for moderately loaded longer spans. Shaikh and Autade (2016) carried out the test on the castellated beam in cantilever action and identified the value of web shear deformation on the critical buckling load of the castellated beam increasing with the increase in cross-sectional area of the tee section and the depth of the web opening. Maraveas et al. (2014) examined several cases of simply supported bridges with different spans and varying widths. This study achieved an optimal design in terms of shape and sizing. Sun et al. (2011) investigated the dynamic characteristics of a 64 m-long steel truss bridge. This study revealed that the expanding heavy-load conditions contributed to the main dynamic performance parameters of bridges, which were slightly larger than conventional conditions.

Many investigations have been done on the structural behavior of truss and castellated beam bridges to date. The structural performance of both bridges, however, has yet to be determined. The pedestrian bridges are evaluated analytically in this paper. Conducting the study, evaluating the internal force to reach the optimal design of bridge components, and watching bridge behavior due to applied loading were all part of this research process.

## 2. RESEARCH METHODOLOGY

There were two types of pedestrian bridges investigated, i.e., the truss bridge (TRB) and the bridge with a deck supported by a castellated beam (CBB). In detail, the bridge geometries are outlined in Figures 1 and 2. The steel grade of BJ-37 was selected for all bridge components. Optimal designs were conducted for the component dimensions. Also, the structural performance of both bridges was investigated.

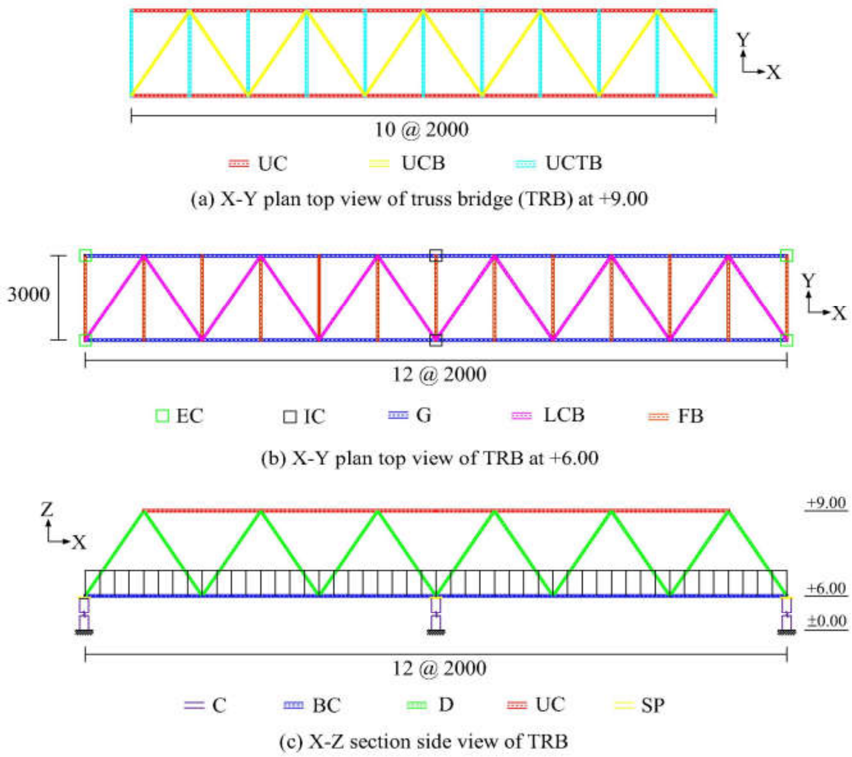


**Figure. 1** Pedestrian truss bridge (unit: mm)

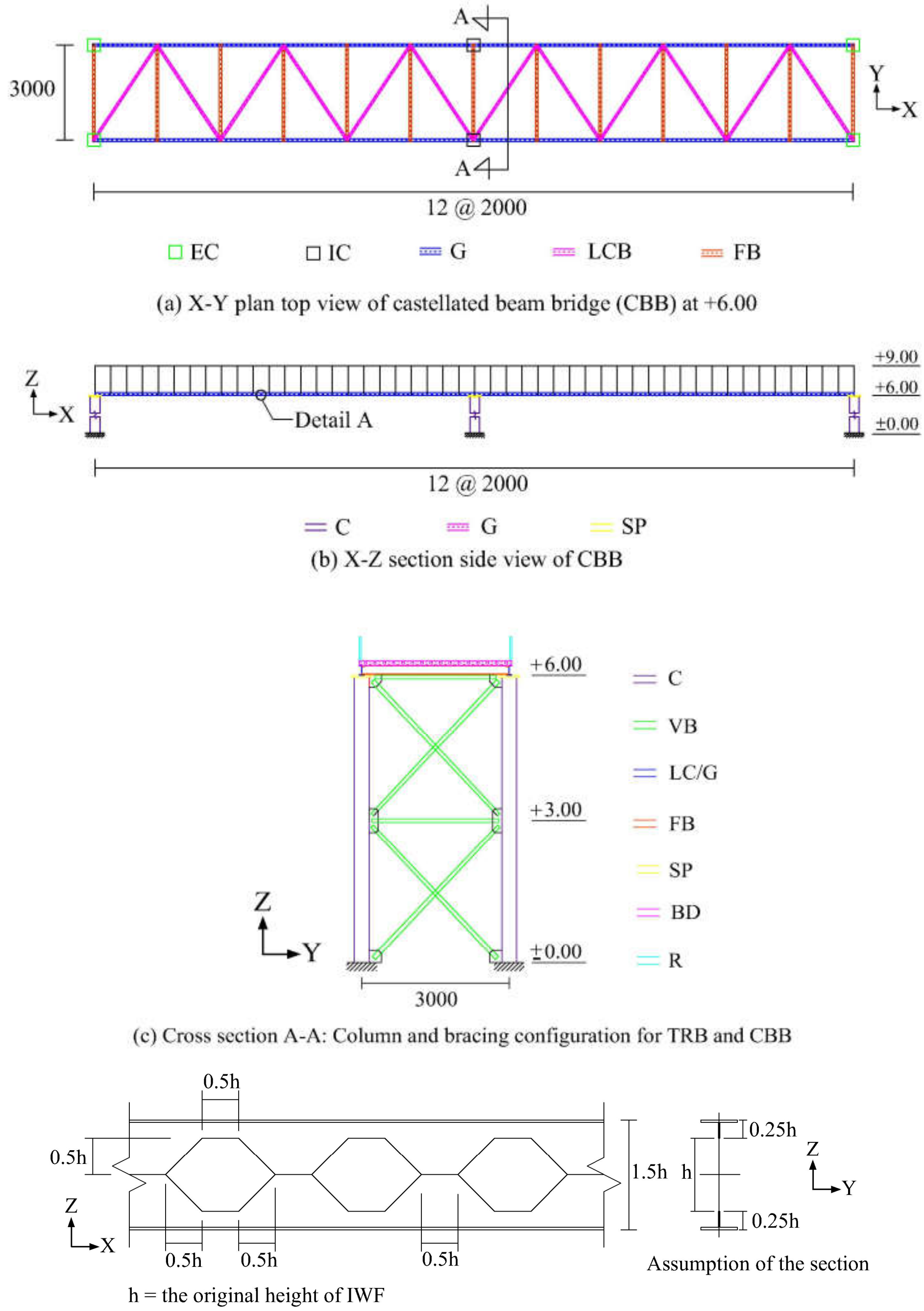


(a) X-Y plan top view of castellated beam bridge (CBB) at +6.00

(b) X-Z section side view of CBB

(c) Cross section A-A: Column and bracing configuration for TRB and CBB

(d) Detail A: Castellated beam

**Figure. 2** Pedestrian castellated beam bridge (unit: mm)

**Table. 1** Bridge components

| No | Component | Abbreviation | No | Component | Abbreviation |
|---|---|---|---|---|---|
| 1 | Internal column | IC | 8 | Diagonal member | D |
| 2 | External column | EC | 9 | Floor beam | FB |
| 3 | Lower chord | LC | 10 | Girder | G |
| 4 | Upper chord | UC | 11 | Bridge deck | BD |
| 5 | Lower chord bracing | LCB | 12 | Railing | R |
| 6 | Upper chord bracing | UCB | 13 | Vertical bracing | VB |
| 7 | Upper chord transverse bracing | UCTB | 14 | Supporting plate | SP |

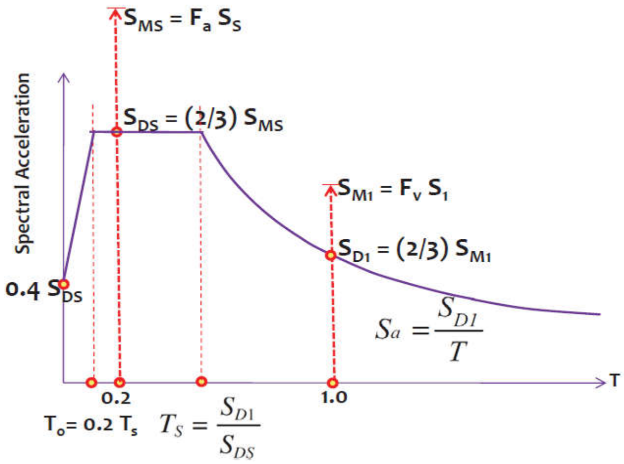


**Figure 3.** Spectral acceleration-period relationship

In a truss bridge, the concrete deck was supported by the bottom chord and floor beam, while in a castellated beam bridge, it was supported by the girder and floor beam. Table 1 shows the components of the bridge. The rigid connection for the truss bridge was allocated to the joint of its components. SAP 2000 v.22 was used to analyze the bridge model for the study. The steel material and load cases for the bridge model were first defined. The load instances were referred to the Panduan Bidang Jalan dan Jembatan (2021). The self-weight of bridges, bridge decks, gusset plates, shear connectors, and railing contributed to the dead loads. The dead loads are 526.95 N and 1251.43 N for connection and railing load, respectively. Each truss joint was subjected to these dead loads. The moving load imposed by pedestrians going across the bridge is known as the live load. 7182 N/m2 was the live load. The wind load is the load that is proportional to the wind pressure operating laterally on the bridge's left and right sides. The wind pressure is calculated depending on the wind speed ($V_{DZ}$).

$$V_{DZ} = 2.5V_0\left(\frac{V_{10}}{V_B}\right) ln\left(\frac{Z}{Z_0}\right) \tag{1}$$

Where $V_{DZ}$ is design wind velocity at design elevation (kms/hour), $V_0$ is the friction velocity, a meteorological wind for various upwind surface characteristics (kms/hour), $V_{10}$ is the wind velocity at 10 meters above low ground or above design water level (kms/hours), $V_B$ is the base wind velocity of 90 to 126 kms/hour at 10 meters height, $Z$ is the height of structure at which wind loads are being calculated as measured from low ground, or from water level, > 10 meters (m), $Z_0$ is friction length of upstream fetch, a meteorological wind characteristic (m)

The design wind pressure ($P_D$) is presented as:

$$P_D = P_B\left(\frac{V_{DZ}}{V_B}\right) \tag{2}$$

Where $P_B$ is the base wind pressure (MPa)

The earthquake load is the lateral load that is unique to a particular area in which SNI-1726-2019 (2019) was used as the load's designation. The bridges were to be built on soft soil in Banda Aceh. As shown in Figure 3, the earthquake load is defined as a response spectrum that forms a relationship between spectral acceleration (Sa) and period (T). The following equations were used to calculate seismic parameters: Spectral acceleration at short periods, $S_{DS}$, and spectral acceleration at a 1-sec period, $S_{D1}$:

$$S_{DS} = \frac{2}{3}S_{MS} \tag{3}$$

$$S_{D1} = \frac{2}{3}S_{M1} \tag{4}$$

Where $S_{MS}$ is the maximum considered spectral acceleration for short periods and $S_{M1}$ is the maximum considered spectral acceleration at 1-sec period.

The bridge model was subjected to several load combinations (C).:

$$C1 = 1.4\ DL \tag{5}$$

$$C2 = 1.2\ DL + 1.6\ LL \tag{6}$$

$$C3 = 1.2\ DL + 1.6\ LL + 0.8\ W \tag{7}$$

$$C4 = 1.2\ DL + 1.3W + 0.5\ LL \tag{8}$$

$$C5 = 1.2\ DL + 1.0\ E + LL \tag{9}$$

$$C6 = 0.9\ DL \pm 1.0\ E \tag{10}$$

Where DL is dead load, LL is live load, W is wind load, E is earthquake load.

The SNI 1729-2020 (2020) was used as the design principle. Table 1 shows the components that were designed for this paper. Out of bracings, all components were wide flange profiles (IWFs). The FB and G were designed under the steel beam principle, with flexural and shear strength verifications performed on these members. The definition of nominal flexural strength (Mn) is:

$$M_n = M_p = F_y Z_x \tag{11}$$

Where $F_y$ is the yield stress (MPa), $Z_x$ is the plastic modulus ($N/mm^3$).

- ❖ If $L_b \leq L_p$, lateral torsional buckling will not be considered.
- ❖ If $L_p < L_b \leq L_r$,

$$M_n = C_b \left[ M_p - \left(M_p - 0.7 F_y S_x\right) \left( \frac{L_b - L_p}{L_r - L_p} \right) \right] \leq M_p \tag{12}$$

- ❖ If $L_b > L_r$

$$M_n = F_{cr} S_x \leq M_p \tag{13}$$

Where $C_b$ is the lateral torsional buckling parameter related to the flexural behavior, $L_b$ is length between points that are either braced against lateral displacement of the compression flange or braced against twist of the cross-section (mm), $L_p$ is the limiting laterally unbraced length for the limit state of yielding (mm), $L_r$ is the limiting unbraced length for the limit state of inelastic lateral-torsional buckling (mm), $F_{cr}$ is critical stress related to the flexural behavior (MPa), $S_x$ is elastic section modulus taken about the x-axis ($mm^3$).

The nominal shear strength in steel ($V_n$) is defined as:

$$V_n = 0.6\ F_y A_w \tag{14}$$

Where $A_w$ is the sectional area of the web ($mm^2$)

Column (C) was designed with considering the bending-axial combination and shear capacity. The nominal compressive strength, $P_n$, is determined as follows:

$$P_n = F_{cr} . A_g \tag{15}$$

Where $F_{cr}$ is the critical stress related to the local buckling verification (MPa), $A_g$ is the gross sectional area ($mm^2$)

Bending-axial combination for column is introduced as follows:

(a) When $\frac{P_r}{P_c} \geq 0.2$

$$\frac{P_r}{P_c} + \frac{8}{9}\left(\frac{M_{rx}}{M_{cx}} + \frac{M_{ry}}{M_{cy}}\right) \leq 1.0 \tag{16}$$

(b) When $\frac{P_r}{P_c} < 0.2$

$$\frac{P_r}{2P_c} + \left(\frac{M_{rx}}{M_{cx}} + \frac{M_{ry}}{M_{cy}}\right) \leq 1.0 \tag{17}$$

Where, $P_r$ is required axial strength (N), $P_c$ is available axial strength (N), $M_{rx}$ and $M_{ry}$ is required flexural strength about x and y-axis (N.m), $M_{cx}$ and $M_{cy}$ is available flexural strength about x and y-axis (N.m).

The LCB, UCB, and UCTB were designed on the principle of compression and tension members. The nominal strength of the compression member is characterized by Eq. (15). The tensile strength, $\varphi_t P_n$, and allowable tensile strength, $P_n/\Omega_t$, of the tension member shall be the lower values obtained according to the limit states of tensile yielding in the gross section and tensile rupture in the net section as expressed in Eqs. (18) and (19).

(a) For tensile yielding in the gross section

$$P_n = F_y A_g \tag{18}$$

$$\varphi_t = 0.90 \text{ (LRFD)} \qquad \Omega_t = 1.67 \text{ (ASD)}$$

(b) For tensile rupture in the net section

$$P_n = F_u A_e \tag{19}$$

$$\varphi_t = 0.75 \text{ (LRFD)} \qquad \Omega_t = 2.00 \text{ (ASD)}$$

Where, $P_n$ is the tensile strength (N), $F_y$ is the yield stress (MPa), $A_g$ is gross sectional area (mm$^2$), $F_u$ is ultimate stress (MPa), $A_e$ is the effective net area (mm$^2$).

The structural capacities of LC, UC, and D were verified to the flexural, shear, and axial strengths due to the rigid connections designed at their ends to ensure those members could resist the bridge loads.

A castellated beam is a beam that has a regular and repeating pattern of hexagonal holes. It is created by cutting the pattern lengthwise across two different halves, offsetting, and then welding them together to create a single expanded beam. A castellated beam is established to increase the beam height so that its flexural capacity can be improved. The details are outlined in Figure 2(d). The inertia is quantified by neglecting the section with the hexagonal opening. In this present paper, the girder was constructed of the castellated beam in which a WF 250 x 250 x 8 x 13 girder was upgraded to be a WF 375 x 250 x 8 x 13 to enhance its flexural strength.

The internal forces, i.e., axial load, shear load, and moment, were contributed by the analysis, and they were used to provide the proper design of both bridges. Additionally, the deformations on the bridge component due to the design implementation were also observed.

The analyses were distinguished between the bridge structure and the column, in which the bridge is located on the top of the column. In the application, the connection between the girder and the top of the column was supposed to be a pin connection so that the main bridge was modeled to be supported by the pins. The column was separately modeled and the pin reactions were transferred to the column as the column load.

## 3. RESULT AND DISCUSSION

### 3.1 The bridge structure

The internal forces, bridge weight, support reactions, and deformation were all discussed throughout the investigation of both bridges. Tables 2 and 3 show the internal forces of both bridges. In general, it was stated that the internal forces of the truss bridge were greater than those of the castellated beam bridge. Lower chords for truss bridges and girders for castellated beam bridges show this tendency more clearly. The weight was expected to be distributed to the joints in the lower chord of a truss bridge, so it was presented as a concentrated load. This joint was attached to the lower chord and the diagonal member, and the joint load was shared fractionally with the diagonal member. Because of this mechanism, the lower chords have substantially fewer internal moments than the girder.

On both bridges, the dimensions of the lower chord and girder as acceptors of loads transferred from the deck were also evaluated. Table 4 summarizes the data for both bridges, including the dimensions of the two components. The table shows that the lower chord sectional area is smaller than the girder sectional area. The lower internal forces performed by truss bridges than those performed by castellated beam bridges may have contributed to this behavior. As illustrated in Table 4, the sectional area of the diagonal member and lower chord of a truss bridge is wider than that of the upper chord. This results implicitly revealed that the diagonal member and lower chord were two main elements which dominantly resisted the bridge load.

**Table. 2** Internal forces and nominal strength for truss bridge

| No | Component | $P_r$ (kN) | $\phi P_c$ (kN) | $M_u$ (kN.m) | $\phi M_n$ (kN.m) | $V_u$ (kN) | $\phi V_n$ (kN) |
|---|---|---|---|---|---|---|---|
| 1 | Lower chord | 16.45 | 444.68 | -13.69 | -59.15 | 12.61 | 219.78 |
| 2 | Upper chord | -78.08 | -181.53 | -2.08 | -27.38 | 2.36 | 149.85 |
| 3 | Lower chord bracing | -3.63 | -87.98 | -2.13E-05 | 0 | -6.51E-05 | 0 |
| 4 | Upper chord bracing | -0.48 | -87.98 | 3.40E-05 | 0 | -3.88E-03 | 0 |
| 5 | Upper chord transverse bracing | -1.69 | -80.68 | 1.92 | 31.46 | -2.07 | -149.85 |
| 6 | Diagonal member | -116.41 | -151.17 | 7.49 | 59.44 | 3.87 | 219.78 |
| 7 | Floor beam | -1.09 | -80.68 | 5.17 | 15.74 | -6.36 | -149.85 |
| 8 | Interior column | -298.26 | -5391.94 | 7.26 | 452.69 | 2.94 | 879.12 |
| 9 | Vertical bracing for interior column | -27.43 | -131.75 | -2.33E-16 | 0 | 1.14E-16 | 0 |
| 10 | Exterior column | -128.14 | -5391.94 | 243.83 | 452.69 | 1.72 | 879.12 |
| 11 | Vertical bracing for exterior column | -15.38 | -131.75 | -2.33E-16 | 0 | 1.14E-16 | 0 |

**Table. 3** Internal forces and nominal strength for castellated beam bridge

| No | Component | $P_r$ (kN) | $\phi P_c$ (kN) | $M_u$ (kN.m) | $\phi M_n$ (kN.m) | $V_u$ (kN) | $\phi V_n$ (kN) |
|---|---|---|---|---|---|---|---|
| 1 | Lower chord bracing | -0.36 | -87.98 | -8.03E-18 | 0 | -2.08E-17 | 0 |
| 2 | Floor beam | -0.52 | -80.68 | 7.90 | 15.58 | 14.03 | 149.85 |
| 3 | Girder | -1.82 | -1009.93 | -261.54 | -333.56 | 84.00 | 539.46 |
| 4 | Interior column | -233.91 | -476.64 | 1.29 | 23.45 | 0.62 | 299.70 |
| 5 | Vertical bracing for interior column | 78.58 | 131.75 | -2.33E-16 | 0 | -4.66E-16 | 0 |
| 6 | Exterior column | -84.73 | -476.64 | 17.21 | 23.45 | 0.62 | 299.70 |
| 7 | Vertical bracing for exterior column | -27.19 | -131.75 | -2.33E-16 | 0 | 1.14E-16 | 0 |

Note: $P_r$ is required axial strength, $\phi P_c$ is the available axial strength, $M_u$ is ultimate bending moment, $\phi M_n$ is the nominal flexural strength, $V_u$ is the ultimate shear force, $V_n$ is the nominal shear strength

**Table. 4** Profile sections of pedestrian bridges

| No | Component | Dimension | |
|---|---|---|---|
| | | Truss bridge | Castellated beam bridge |
| 1 | Lower chord | WF 200 x 100 x 5,5 x 8 | - |
| 2 | Upper chord | WF 150 x 75 x 5 x 7 | - |
| 3 | Lower chord bracing | L 100 x 100 x 10 | L 100 x 100 x 10 |
| 4 | Upper chord bracing | L 100 x 100 x 10 | - |
| 5 | Upper chord transverse bracing | WF 150 x 75 x 5 x 7 | - |
| 6 | Diagonal member | WF 200 x 100 x 5,5 x 8 | - |
| 7 | Floor beam | WF 150 x 75 x 5 x 7 | WF 150 x 75 x 5 x 7 |
| 8 | Girder | - | CB WF 375 x 250 x 8 x 13 |
| 9 | Bridge deck | t = 100 mm | t = 100 mm |
| 10 | Railing | Dia. 75 mm | Dia. 75 mm |
| 11 | Supporting plate | t = 10 mm | t = 10 mm |
| 12 | Interior Column | WF 400 x 400 x 11 x 18 | WF 250 x 125 x 6 x 9 |
| 13 | Vertical bracing for interior column | L 120 x 120 x 12 | L 120 x 120 x 12 |
| 14 | Exterior column | WF 400 x 400 x 11 x 18 | WF 250 x 125 x 6 x 9 |
| 15 | Vertical bracing for exterior column | L 120 x 120 x 12 | L 120 x 120 x 12 |

Note: CB is castellated beam

The truss bridge also noticeably performed with a smaller deflection than that of the castellated beam bridge, as shown in Table 5. Namely, the truss configuration diminishes the deflection by up to 517.9% when it is confirmed to the castellated beam bridge. In a truss bridge, the diagonal members were one of the elements connected to the truss joint and it was possible to receive a partial transferred load as previously explained. Due to the load sharing, the deflection on the truss bottom chord is possible to deduct. On the contrary, the castellated

**Table. 5** Deflection on the bridge

| No | Bridge type | Deflection (mm) |
|---|---|---|
| 1 | Truss bridge | -7.08 |
| 2 | Castellated beam bridge | -43.74 |

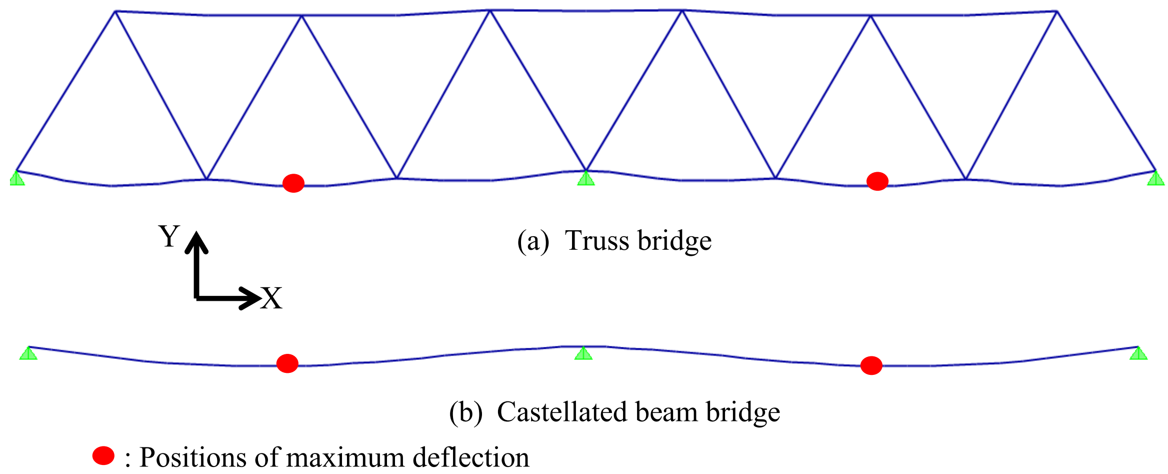


**Figure. 4** Deflection patterns on both bridges

beam bridge employed a girder with hexagonal openings on the web. Hence, the girder inertia is reduced at the designated positions due to the web openings. Due to several openings, the deflection on the bridge girder becomes greater than that on the truss bottom chord. Additionally, the deflections on truss and castellated beam bridges were indicated to be less than 50 mm, which is the allowable deflection of both bridge models. The maximum deflection for both bridges is indicated at the middle position for each span, as illustrated in Figure 4.

Table 6 demonstrates the components and total weight of both bridges. This table indicates the heavier main bridge and columns on the truss bridge than on the castellated beam bridge. The difference in the total weight of the two bridges is identified to be 17.4%. More components that support the truss bridge are expected, which is why the truss configuration is heavier than the castellated beam bridge. Thus, the greater support reaction in the truss was performed due to the heavier structure.

Furthermore, observations on the bridge reactions were also carried out. Those reactions are expressed in Table 7, which illustrates the higher vertical and horizontal reactions on the truss bridge than on the castellated beam bridge. The higher vertical support reactions on truss bridges were demonstrated due to the heavier dead load resulting from the self-weight. The vertical support reaction disparity of both bridges is specified to be 4.7% on the interior column positions and 18.7% on the exterior column positions, respectively. Observation of horizontal reactions also revealed the truss bridge performed higher reactions than the castellated beam bridge. The difference in horizontal reactions was 43.1% on the interior and 46.9% on exterior column spots. This distinction is supposedly made due to the catchment area of wind on the truss bridge, which is identified to be wider than that of the castellated beam bridge. Thus, the horizontal base reaction becomes greater in a truss bridge.

.

### 3.1 The column structure

As formerly outlined in Figures 1(b) and 2(c), the main body of the bridge is supported by six columns. The diagonal bracings are constructed in that configuration to maintain the column's position. The columns were distinguished by their location on the bridge span, i.e., interior and exterior columns, respectively. Table 6 explains that the truss columns are heavier than those of castellated beam bridges due to the larger sectional area of the components.

**Table. 6** Weight of pedestrian bridges

| No | Bridge type | Element | Weight (ton) | |
|---|---|---|---|---|
| | | | Per component | Total |
| 1 | Truss bridge | Main bridge | 22.32 | 26.69 |
| | | Interior column | 2.18 | |
| | | Exterior column | 2.18 | |
| 2 | Castellated beam bridge | Main bridge | 21.09 | 22.73 |
| | | Interior column | 0.82 | |
| | | Exterior column | 0.82 | |

**Table. 7** Support reactions of the main bridge

| No | Bridge type | Component | Fx | Fy | Fz |
|---|---|---|---|---|---|
| | | | kN | kN | kN |
| 1 | Truss bridge | Interior column | 2.87E-06 | -9.74 | 260.65 |
| | | Exterior column | 40.64 | -7.31 | 90.80 |
| 2 | Castellated beam bridge | Interior column | 2.10E-12 | -6.81 | 248.98 |
| | | Exterior column | 2.88 | -4.97 | 76.52 |

**Table. 8** Support reactions of the bridge column

| No | Bridge type | Component | $F_x$ | $F_y$ | $F_z$ | $M_x$ | $M_y$ | $M_z$ |
|---|---|---|---|---|---|---|---|---|
| | | | kN | kN | kN | kN.m | kN.m | kN.m |
| 1 | Truss bridge | Interior column | -21.89 | -2.87E-06 | 318.11 | 1.72E-05 | -7.26 | 2.79E-09 |
| | | Exterior column | -12.04 | -40.64 | 139.34 | 243.85 | -4.61 | 0.04 |
| 2 | Castellated beam bridge | Interior column | -49.92 | -2.10E-12 | 284.10 | 1.26E-11 | -1.29 | 6.52E-14 |
| | | Exterior column | -19.04 | -2.88 | 104.40 | 17.27 | -0.60 | 0.09 |

**Table. 9** Lateral deformation for truss and castellated beam bridge

| No | Bridge type | Component | Lateral deformation (mm) |
|---|---|---|---|
| 1 | Truss bridge | Interior column | 0.38 |
| | | Exterior column | 0.27 |
| 2 | Castellated beam bridge | Interior column | 0.59 |
| | | Exterior column | 0.39 |

Table 7 presents the support reactions of the main bridge as the load is distributed from the main bridge to the column. The greater support reactions, particularly in the vertical direction (z-axis), are expressed by the truss bridge due to the self-weight of several steel components establishing the truss bridge. The column base reactions are shown in Table 8. The table shows the vertical support reactions on the column of the truss bridge are greater than those of the castellated beam bridge. The differences in vertical reactions are 11.9% for interior and 33.5% for exterior columns. This behavior is possibly exhibited since the column of a truss bridge receives a higher gravity load from the bridge support on the interior than that on the exterior column.. Additionally, the greater horizontal reaction on the truss bridge than that of the castellated beam also contributed. The result is allegedly due to the higher horizontal load applied to the truss column's upper side.

The lateral deformations on column for both bridges were also observed. As illustrated in Table 9, the smaller lateral deformation on truss column than that of the castellated beam bridge is figured out. The disparity of 56 %

https://doi.org/10.24815/jarsp.v5i2.25766

and 42.1 % on lateral deformation are expressed for interior and exterior columns, respectively. The column of the truss bridge which has a wider sectional area is highly expected to be more able to resist the lateral deformation. Meanwhile, the column on the castellated beam bridge was designed in a smaller sectional area so that when the lateral load acted on that column, it will be significantly deformed.

## 4. CONCLUSION

This study compared the structural performance of two types of pedestrian bridges, a truss bridge, and a castellated beam bridge, based on their configuration. Both bridges were intended to present the bridge performance in the best possible way. In general, the internal force and deflection of the truss bridge were lower than those of the castellated beam bridge. The truss bridge, however, was significantly heavier than the castellated beam bridge. For main bridges and columns, observation of the support revealed that the truss bridge produced greater support reactions than the castellated beam bridge. These behaviors were allegedly pointed out as a result of the truss bridge's heavier construction. The greater support reaction on the truss bridge leads to a bigger foundation plate than that of the castellated beam bridge. Based on this present study, it is suggested to utilize the castellated beam configuration for pedestrian bridges due to the lighter weight of construction that can ensure the safety and economical aspect of the bridge structure.

## REFERENCES


Ali, S., Thambiratnam, D., Liu, X., Fawzia, S. 2020. Numerical study of pedestrian suspension bridge with innovative composite deck. *Heliyon*, 6 (2020), pp. 1-12

Belykh, I., Jeter, R., Belykh, V. 2017. Foot force models of crowd dynamics on a wobbly bridge. *Science Advance*, 3, pp. 1-12.

Chang-jun, Z., Dai-ping, C., Xiao., Q., Chang-sheng, Z. 2011. Research on reasonable structure forms of pedestrian suspension bridges. *Huazhong University of Science & Technology*, pp. 613-616.

Dey, P., Walbridge, S., Narasimhan, S. 2015. Vibration serviceability analysis of aluminum pedestrian bridges subjected to crowd loading. *6th International Conference on Advances in Experimental Structural Engineering*, August 1-2, 2015, University of Illinois, Urbana-Champaign, United States

Kustura, M., Šunjić, G., Šunjić, B. 2020. Pedestrian bridges and load testing. *Electronic collection papers of the Faculty of Civil Engineering*, 19 (2020), pp. 88-102.

Li, J., Jia, L., Shujin, L., Baifeng, J., Youfu, D. 2013. Simulation for wind pressure of pedestrian bridge induced by main line train. *Applied Mechanics and Materials*, 423-426 (2013), pp. 1268-1271

Li, M. 2011. Study on Dynamic Test of a Large Span Steel Truss Pedestrian Bridge. *Advanced Materials Research*, 225-260 (2011), pp.769-775

Maraveas, C., Papagiannakis, A., Miami, K., Tasiouli, K. 2014. Optimal design of through-truss steel bridges. *WIT Transactions on The Built Environment*, 137, pp. 465-476.

Panduan Bidang Jalan dan Jembatan 2021. Perencanaan Praktis Perencanaan Teknis Jembatan, pp. 1-1537.

Shaikh, A.S., Autade, P. B. 2016. Structural analysis and design of castellated beam in cantilever action. *International Research Journal of Engineering and Technology*, 3(8), pp.163-170.

SNI- 1729-2020. Spesifikasi untuk bangunan gedung baja struktural, pp. 1-311.

SNI-1726-2019. Tata cara perencanaan ketahanan gempa untuk struktur bangunan gedung dan nongedung, pp. 1-254.

Sophocleous-Lemonari, A., Michael, A., Phocas, M.C. 2013. Hybrid structures. A case of pedestrian bridge. *Second international Conference on Structures and Architecture*, July 24-26, 2013, Guimaraes, Portugal.

Sun, Z., Shen, J., Zhao, J., Su, Z. 2011. Study on dynamic characteristic of 64m railway steel truss bridge on expanding heavy-load transport condition. *Applied Mechanics and Materials*, 90-93(2011), pp. 1100-1105.

Tej, P., Tejová, A., Kolísko, J. 2014. Design of an experimental tensegrity pedestrian bridge. *Applied Mechanics and Materials*, 587-589 (2014), pp. 1646-1649.

Wakchaure, M.R., Sagade A.V., Auti, V. A. 2012. Parametric study of castellated beam with varying depth of web opening. *International Journal of Scientific and Research Publications*, 2(8), pp. 1-6